

NDVI anomaly patterns over Africa during the 1997/98 ENSO warm event

A. ANYAMBA, C. J. TUCKER,

NASA/Goddard Space Flight Center, Biospheric Sciences Branch, Code 923.0,
Greenbelt, MD 20771, USA; e-mail: assaf@cerrado.gsfc.nasa.gov

and J. R. EASTMAN

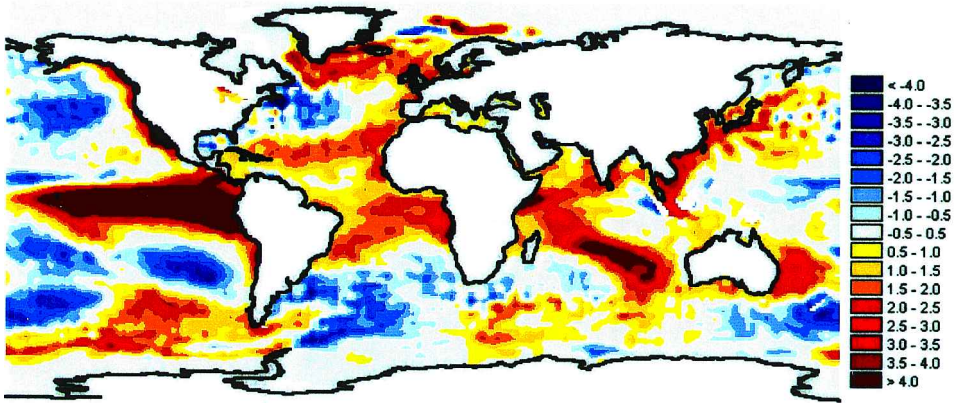
Clark University, Graduate School of Geography, 950 Main 3, Worcester,
MA 01610, USA

(Received 26 May 1999; in final form 28 June 2000)

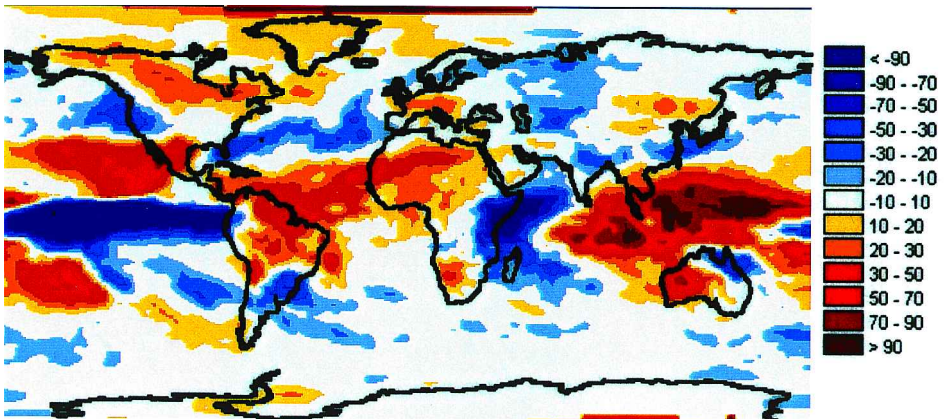
Abstract. Normalized Difference Vegetation Index (NDVI) departure patterns for Africa during the 1997/98 El Niño/Southern Oscillation (ENSO) warm event show two dominant patterns. Over equatorial Eastern Africa, above normal NDVI anomalies persisted from October 1997 through the normal dry season (December–February) and into the long rains season in March–May. Over Southern Africa the spatial NDVI anomaly shows a dry western half and a relatively greener than normal eastern half. Correlations between the temporal NDVI anomalies with ENSO indices shows that the anomalous conditions over Eastern Africa were a direct result of anomalous warming of sea surface temperatures ($\sim +3^{\circ}\text{C}$) in the western equatorial Indian Ocean (WIO) and a lagged response to the warming in the eastern Pacific Ocean ($+4^{\circ}\text{C}$). We suggest that this anomalous warming of the WIO and the equatorial eastern Atlantic Ocean basin dampened the normal severe drought response pattern over Southern Africa where mild drought conditions were experienced. The overall continental response pattern shows a meridional dipole pattern, with above normal NDVI straddling the equator between 10°N and 10°S and normal to slightly below normal NDVI south of 15°S , predominantly over south-western Africa.

1. Introduction

During the period June 1997 to May 1998, the global climate system was perturbed by the largest El Niño/Southern Oscillation (ENSO) phenomenon observed this century (McPhaden 1999). Anomalous warming in the eastern Pacific Ocean reached a record $+4^{\circ}\text{C}$ as seen in figure 1(a). The effect of this warming was illustrated by the shift in the belt of maximum tropical deep convection from the western Pacific region to the central and eastern Pacific regions as inferred from outgoing longwave radiation (OLR) data (figure 1(b)). This shift resulted in above normal rainfall over the eastern Pacific islands, Peru, extending into the extra tropics to affect California, and the US Gulf States. On the western side of the Indian Ocean, extremely elevated levels of rainfall fell over much of Eastern Africa. On the other hand, Indonesia, north-east Brazil, Hawaii and Papua New Guinea experienced



(a)



(b)

Figure 1. (a) Composite SST anomalies ($^{\circ}\text{C}$) for December–February 1997/98. The pronounced dipole pattern between the western Pacific (cold, negative SSTs) and the central-eastern Pacific (warm, positive SSTs) is a typical occurrence during ENSO warm events. Note also the warmer than normal SSTs in the WIO ($> +3^{\circ}\text{C}$) and in the equatorial South Atlantic Ocean ($\sim +2^{\circ}\text{C}$). Departures in SST are calculated with respect to 1982–1998 means. (b) Composite Outgoing Longwave Radiation (OLR) anomalies (W m^{-2}) for December–February 1997/98. Positive anomalies indicate dry conditions while negative departures indicate areas of deep, cold clouds where precipitation is likely to occur. Note the east–west dipole pattern of negative (east, wet) vs. positive (west, dry) across the Pacific basin. Over Africa there is a marked meridional difference in the departures, with negative anomalies over East Africa indicative of intense convective activity and positive anomalies covering the western half of Southern Africa indicative of dry conditions.

unprecedented drought that precipitated outbreaks of forest fires, especially in Indonesia and Brazil. This event was in many ways a classic illustration of the teleconnection patterns resulting from the interannual reversal in the Tropical Walker Circulation system. The rainfall anomalies observed during this event closely follow the results from a study by Ropelewski and Halpert (1987, 1996).

In this study we analyse and describe the biosphere response to these anomalous

climatic conditions using normalized difference vegetation index (NDVI) data for Africa for the period July 1997 to May 1998. The index is derived from broad band measurements in the visible and infrared channels made by the Advanced Very High-Resolution Radiometer (AVHRR) instrument onboard the National Oceanographic and Atmospheric Administration (NOAA) series of polar orbiting meteorological satellites. The index is calculated as $NDVI = (Ch2 - Ch1) / (Ch2 + Ch1)$ where $Ch1$ and $Ch2$ are upwelling land surface radiances in the red and near-infrared wavelengths, respectively. It has been found to provide a strong vegetation signal and good spectral contrast from most background materials (Tucker and Sellers 1986), with restrictions in some arid and semi-arid areas where bare soil reflectance may cause large NDVI variations (Huete and Tucker 1991, Farrar *et al.* 1994). It has also been shown to be a good indicator of various vegetation parameters including green leaf area index (LAI), biomass, percentage green cover, green biomass production and the fraction of absorbed photosynthetically active radiation (Tucker 1979, Sellers 1985, Asrar 1989). Taken as time-series measurements, NDVI is well correlated with climate variables including rainfall and evapotranspiration in a wide range of environmental conditions (Gray and Tapley 1985, Justice *et al.* 1986, Nicholson *et al.* 1990, Cihlar *et al.* 1991). NDVI may therefore be considered to represent the integration of the land surface responses to climate variability at various time and space scales. Employing various data decomposition techniques, it has been illustrated recently that seasonal scale signals (Eastman and Fulk 1993, Andres *et al.* 1994) and interannual signals are related to ENSO (Eastman and Fulk 1993, Myneni *et al.* 1995, Anyamba and Eastman 1996). Furthermore, examination of monthly NDVI anomaly patterns shows that there are unique land surface response patterns from one ENSO warm event to another (Eastman and Anyamba 1996). In totality, NDVI can be used as an indicator of the biosphere response to climate variability at a range of time scales.

2. Data and analysis methods

The Global Inventory Monitoring and Modeling Systems (GIMMS) group at NASA/GSFC processed the NDVI data used in this analysis. Near-real time data processing for Africa is carried out to support the activities of the United States Agency for International Development (USAID) Famine Early Warning System (FEWS) project. The data, at 8 km spatial resolution, are first processed as 10-day composites using the maximum value compositing procedure to minimize effects of cloud contamination (Holben 1986, Tucker and Newcomb 1994). For the purpose of this research, we created monthly composites from three 10-day composites in any given month to further minimize the effects of clouds on the vegetation signal and to match the monthly temporal resolution of the associated ENSO indices. In addition, calibration based on invariant desert targets has been applied to the data to minimize the effects of sensor degradation (Los 1993). The time series of these measurements began in July 1981 and continues to date. So far it constitutes the longest available representation of global biosphere dynamics for studies of climate-vegetation interactions (Los *et al.* 1994). The ENSO indices used in the analysis include the following.

1. Sea surface temperatures (SST) anomaly data drawn from the NINO3.4 ENSO monitoring region in the eastern Pacific Ocean ($5^{\circ}N-5^{\circ}S$; $170-120^{\circ}W$).

2. The Southern Oscillation Index (SOI), which represents the basin-wide see-saw in atmospheric pressure patterns between the eastern and western Pacific, measured as normalized difference in sea level pressure between Papeete, Tahiti, and Darwin, Australia.
3. The Eastern Pacific Wind Index (EPWI) (5°N – 5°S ; 135 – 120°W), which represents the interannual variability in the wind flow patterns in the eastern Pacific region.
4. The equatorial Western Indian Ocean (WIO) SST index (10°N – 10°S ; 40 – 64°E), which was extracted from the gridded global SST time series dataset. The region selected for computation of this index (excluding land areas) showed the largest magnitude of positive SST departures in the WIO during the 1997/98 ENSO event. It is more or less similar to the domain used by Saji *et al.* (1999) in the computation of an east–west dipole index for the Indian Ocean.

Other indicators of tropical interannual climate dynamics used in this analysis include variations in the North Atlantic SST [NAT] (5 – 20°N , 60 – 30°W), South Atlantic SST [SAT] (0 – 20°S , 30°W – 10°E), Global Tropics SST [TROP] (10°S – 10°N , 0 – 360°) and the Quasi-Biennial Oscillation Index (QBO30) of zonally averaged winds at 30 MB over the equator. Variations in patterns of SSTs in the Atlantic have an influence on the location and intensity of the Intertropical Convergence Zone and hence on precipitation over Africa (Lamb *et al.* 1986, Hastenrath 1990). All the ENSO and tropical SST indices were obtained from the active archive of NOAA's Climate Prediction Center (CPC).

NDVI anomaly images were computed as differences from monthly long-term means using the 17-year record (1982–1998 used as the base period), excluding cloud pixels. Though this period of anomaly analysis is relatively short and characterized by some discontinuities in the mapping instruments (Kaufman and Holben 1993), the results obtained agree well with the departure patterns in both OLR (figure 1(b)) and in rainfall as illustrated in Bell and Halpert (1998). The NDVI anomaly patterns for the period September 1997 to April 1998 are shown in figure 2. The nature of the general teleconnections between ENSO and patterns of variability in NDVI over Africa is explored using correlation and cross-correlation analysis techniques (Katz 1988) between NDVI anomalies at selected sites and ENSO indices. Three sites were sampled for use in the correlation analysis. For each site, box averages of the long-term means, monthly values and monthly anomalies were computed from a $100\text{ km} \times 100\text{ km}$ area centred on each of these locations. For East Africa, the sample site is located in eastern Kenya centred at 40°E , 0°S , with two sites in Southern Africa, in Namibia (18°E , 22°S) and South Africa (29°E , 29°S). These sites were selected taking into account the areas that show anomalous precipitation response to ENSO (Ropelewski and Halpert 1987, 1989, 1996, Nicholson and Kim 1997) and the observed anomaly patterns in NDVI during this event and during previous ENSO warm events (Myneni *et al.* 1995, Eastman and Anyamba 1996).

3. Results

3.1. Spatial evolution of NDVI anomaly patterns

Monthly NDVI anomalies for the 1997/98 ENSO warm event from September 1997 to April 1998 are shown in figure 2. Anomalies are computed in NDVI units (NDVI range -1 to $+1$). September 1997 shows a discontinuous band of negative

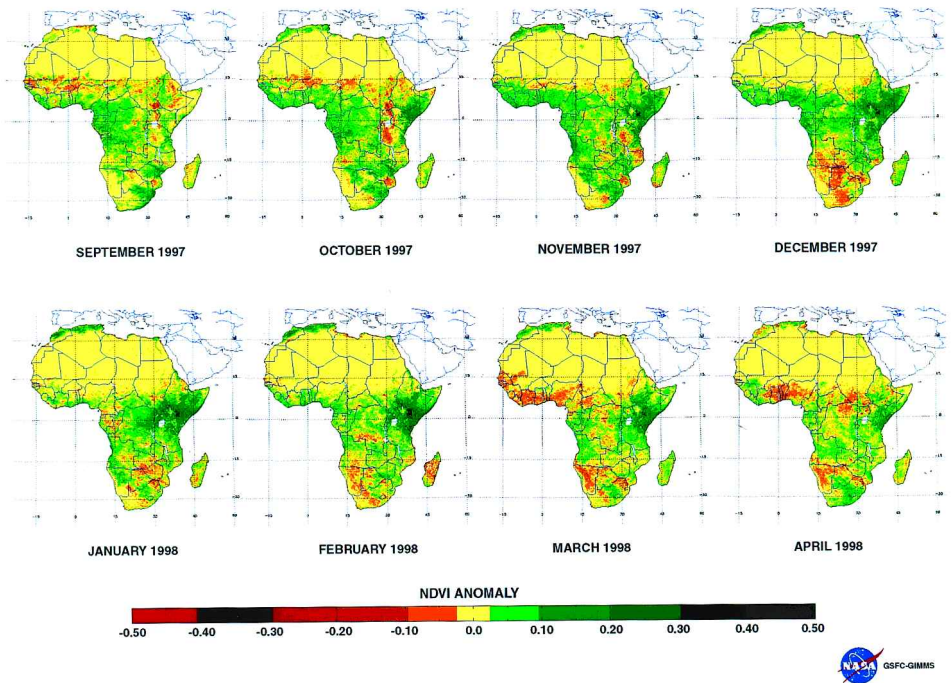


Figure 2. Monthly AVHRR NDVI anomaly images of continental Africa during the 1997/98 ENSO warm event (September 1997–April 1998). Departures are calculated with respect to 17-year means (1982–1998). Green areas show positive NDVI anomalies, yellow, neutral, and brown-red show negative NDVI anomalies. Positive anomalies in East Africa during the entire period correspond well with the location of negative anomalies in OLR shown in figure 1(b). Negative departures are observed in the western half of Southern Africa in December 1997 and from February to April 1998.

NDVI anomalies across the Sahel into parts of East Africa and positive anomalies along the West African coastal belt, the Congo Basin region, and south-eastern Africa. September is for the most part a transitional month, when the rains recede from the Sahel with the movement of the Intertropical Convergence Zone (ITCZ) from the Northern hemisphere to the Southern hemisphere over the continent. The first strong indicator of anomalous conditions occurs in October. Positive anomalies in NDVI (~ 0.2) occur in East Africa predominantly in areas east of the Rift Valley, covering the coastal plain lands and semi-arid and arid areas of eastern and north-eastern Kenya and Somalia. The western half of East Africa shows negative NDVI anomalies, resulting in a zonal east (positive)–west (negative) anomaly in vegetation conditions. Isolated clusters of positive NDVI anomalies occur in south-eastern Africa. The positive anomaly pattern over Kenya and Somalia is enhanced in November–December ($> +0.20$) as the short rains season progresses to cover most of East Africa extending westwards into Uganda, the Congo Basin region, Cameroon and northwards into Ethiopia, an area approximately bounded by 10° N and 10° S.

The above normal NDVI across the equatorial belt of Africa was a result of enhanced convective activity within the ITCZ (figure 1(b)) due to elevated SSTs in both the equatorial WIO and the equatorial southern Atlantic Ocean (figure 1(a)). Strong positive anomalies occur along the West Africa coast southwards to Angola

and in North Africa over Morocco and Algeria. Lamb and Pepler (1991) have shown that variability in Moroccan rainfall between November and April is related to the state of the North Atlantic Oscillation (NAO) and weakly related to ENSO. The NAO is an interannual climate variability signal measured by the pressure difference between the region surrounding Iceland and the region around the Azores Islands, north-west of Morocco in the Atlantic Ocean. The observed NDVI anomalies over north-western Africa during this period may thus be a result of the interaction of these two phenomena.

At a continental scale, December 1997 shows a meridional dipole in NDVI patterns. A band of positive NDVI anomalies stretches across Africa between approximately 12°N and 10°S . The area south of 10°S shows negative NDVI anomalies (-0.1 to -0.2) primarily in Botswana, north-eastern Namibia, southern Angola and southern Zambia. The positive NDVI anomaly patterns over the entire eastern Africa region persist through February 1998. The area of high positive anomalies is reduced by March and April, primarily covering Kenya and central to southern Somalia, while negative NDVI anomalies emerge along the west African coastal strip and over the western half of East Africa. Over southern Africa the negative NDVI anomalies become more marked in March–April. The spatial structure shows a north-west (negative) and south-east (positive) dipole pattern in March and April. This pattern is somewhat similar to that observed during the 1986/87 and 1994/95 ENSO warm events over the region and represents one of the two types of ENSO spatial manifestation identified in Southern Africa using NDVI data (Eastman and Anyamba 1996). One of the most significant manifestations of the 1997/98 ENSO warm event is the persistence and extension of positive NDVI anomalies from the short rains growing season (October–December) into the dry season (January–February) and into the long rains season (March–June) over eastern Africa. As such there was no dry period experienced early in 1998 which was quite a dramatic departure from the normal seasonal cycle. In general, the continental-scale patterns of NDVI anomalies correspond well with rainfall teleconnections patterns as shown in Ogallo (1988) and Ropelweski and Halpert (1987), with a somewhat limited drought extent over Southern Africa. The classic ENSO teleconnection pattern over Africa is the tendency for equatorial East Africa to receive above normal rainfall and for drought to persist over Southern Africa during ENSO warm events (Lindsey 1988).

3.2. Temporal evolution of NDVI means and anomalies

Three sites were selected for analysis of the temporal evolution of NDVI means and anomalies. Plots of the long-term means, monthly means and anomalies for these sites are shown in figure 3(a–f). The East Africa site (figure 3(a)) shows a dramatic increase in NDVI from September to October 1997 reaching a maximum in February 1998 and decreasing to near previous October 1997 levels by April–May 1998. The evolution of the anomalies (figure 3(d)) shows a normal curve pattern centred on December/January, and is very typical of the phase locking character of ENSO to the SST annual cycle in the eastern Pacific Ocean (Rasmusson and Carpenter 1982). The NDVI levels for the period October to March are much higher than the long-term average (figure 3(a)). As can be noted, the typical low NDVI levels during the dry season over the region during December–February were not observed. As a result the region experienced continuous above normal NDVI levels for a period of 8 months from October 1997 to May 1998 (figure 1). This was a

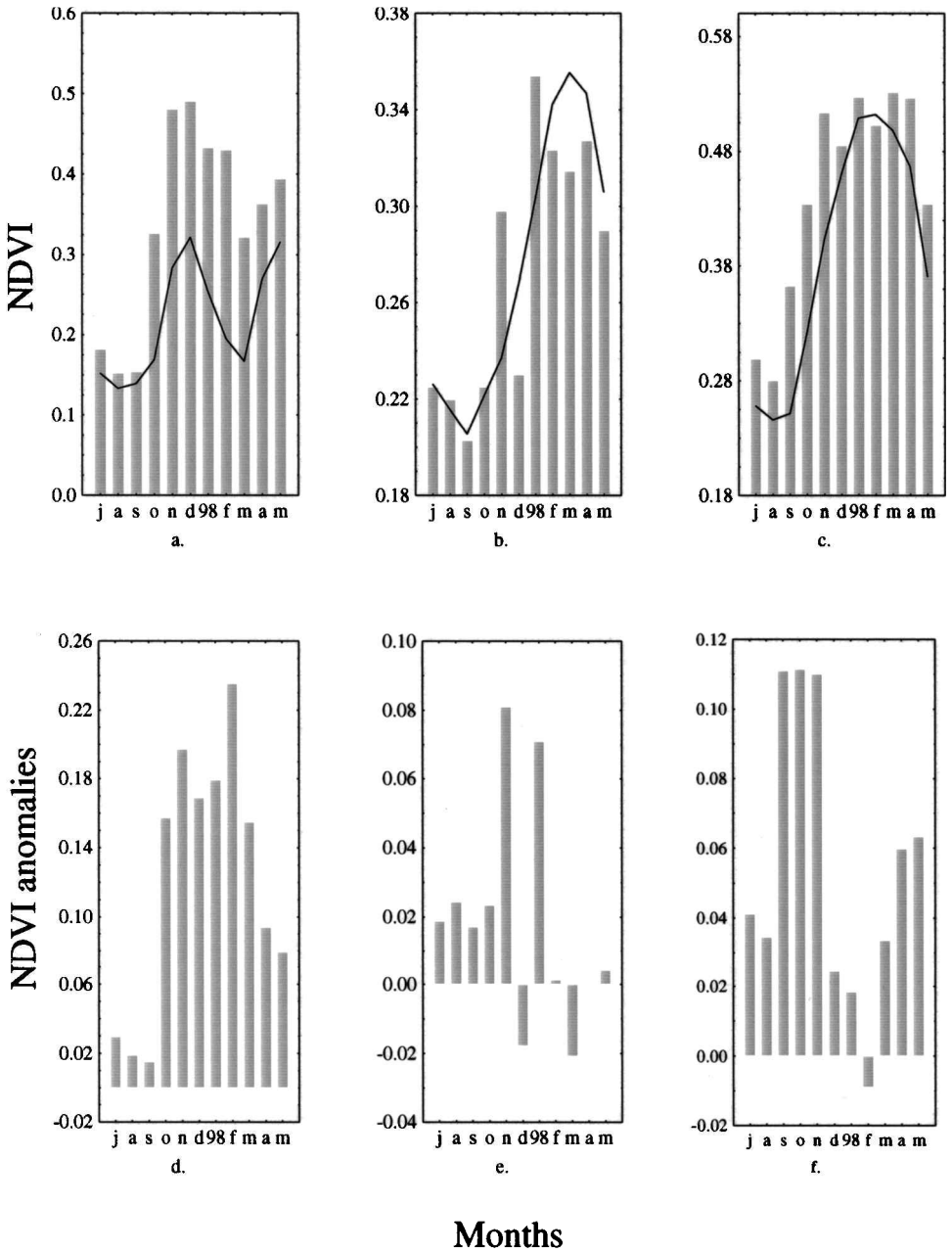


Figure 3. Temporal profiles of monthly NDVI values and long-term means (top panel) for (a) East Africa (40° E, 0° S), (b) Namibia (18° E, 22° S) and (c) south-eastern South Africa (29° E, 29° S). The corresponding NDVI anomalies for these sites are shown in the bottom panel (d, e, f). Black line plots are long-term mean values, grey bars are monthly values and anomalies. The NDVI values are averages extracted from a 100 km × 100 km box centred on each of these locations. For East Africa during the period July 1997–May 1998, the NDVI anomalies are well above the long-term means (d) indicative of greener than normal conditions. For the Southern Africa sites (e, f), the anomalies are above their respective long-term means during the early part of the growing season (September–November) and near normal or slightly below normal during the peak growing season (December–March).

result of the record breaking, above normal rainfall received during this period; some areas in coastal, central and eastern Kenya and in Somalia averaged 5–10 times the normal rainfall (Bell and Halpert 1998).

The temporal profile drawn from Namibia shows a slight decrease in NDVI from July to September then an increase to values above the long-term mean in November 1997 during the Southern hemisphere spring season (figure 3(b)). This is followed by a dramatic decrease in December 1997 below the long-term mean, then an increase to just above the long-term mean values in January 1998. The later part of the growing season (February to May) shows slightly below normal NDVI, with the maximum negative anomaly in March 1998 (figure 3(e)). One noticeable feature of the anomalies is the increase in NDVI prior to the beginning of the growing season (September–November) and a decrease in December. This character has been noted as a precursor during warm ENSO years (Eastman and Anyamba 1996). This pattern is consistent with the tendency for above normal precipitation over the region during the early phase of a developing warm event and lower than normal precipitation during the mature phase of a warm event (Diaz and Kiladis 1993, Nicholson and Entekhabi 1986). Long-term means and monthly NDVI values from the second site in south-eastern South Africa are shown figure 3(c). The annual cycle defined by the long-term average shows a minimum in NDVI during September and a maximum in February. The corresponding monthly NDVI values during the period of analysis follow a similar pattern. The earlier part of the growing season (September–November) shows significantly above normal NDVI decreasing to slightly below normal conditions in February 1998 and a recovery to slightly above normal conditions from March to May (figure 3(f)). Overall, the drought conditions were not as severe over the Southern Africa region as in previous ENSO warm events. The western portions of the region were slightly drier than normal, especially in Namibia and northern Botswana in December, February–April (figure 2) as compared with the south-eastern region covering the Drakensburg Mountains and parts of Transvaal which were greener than normal. The dominant regional pattern over Southern Africa shows a north-west (negative)–south-east (positive) dipole pattern in NDVI anomalies. This pattern supports findings by Eastman and Anyamba (1996) of the different manifestations of ENSO warm event teleconnection patterns over Southern Africa. This north-west–south-east spatial pattern is also well marked in the OLR anomalies (figure 1(b)).

3.3. Correlation patterns between NDVI anomalies and ENSO indices

In the context of ENSO, teleconnections in global weather patterns are based on the notion that there is a tendency for anomalous warming in SSTs in the eastern Pacific Ocean (figure 1(a)) to have widespread impacts over distant or remote locations. Specifically, this is manifested in the amplification/dampening of the precipitation signal (and hence vegetation greenness patterns in our case) over widespread locations over the global tropics. The Pacific signal is transmitted via the Atmospheric Walker Circulation System (Southern Oscillation) causing dramatic changes in the normal patterns of precipitation in the major centres of tropical convection including the Amazon Basin, Indonesia and Congo Basin and the surrounding areas (figure 1(b)). These changes result in above normal precipitation in some regions and below normal precipitation in others. Typically, anomalous conditions associated with ENSO are observed during the rainfall/growing season for specific tropical locations. To test whether there is any correlation between NDVI departure patterns

over Africa and ENSO during the 1997/98 period, we computed correlations between ENSO indices and NDVI anomalies for selected sites (in §3.1 above) in East and Southern Africa.

The evolution of NDVI anomalies over eastern Kenya compared with the SST anomalies in the adjacent region in the WIO is shown in figure 4(a) for the period July 1997 to May 1998. As can be seen, the patterns of evolution of the two variables co-evolve well with a peak in January (WIO-SST) and February (NDVI) and a drop in the anomalies towards the end of the long rains growing season in May. For the entire time period both the NDVI and SST show positive anomalies. There is no apparent lag relationship except for the peak period in the series, where the SST reaches a maximum in January and the NDVI reaches a maximum in February. Simultaneous variations between NDVI and SST are observed; nevertheless NDVI attests to a time response of 1–2 months in the semi-arid lands of Africa (Nicholson *et al.* 1990, Richard and Pocard 1998). The coefficient of correlation between the two time series is 0.83 ($p < 0.005$). This shows the close coupling between WIO warming, precipitation and vegetation greenness patterns over large areas of East Africa during this period. Significant correlations are also found with the global tropical SSTs (0.87) and the Southern Atlantic SSTs (0.83) (table 1). This in part shows the influence of an enhanced ITCZ due to above normal SST across the global tropics and its effects on precipitation (figure 1(a)) and thus vegetation over East Africa (figure 2).

Lag correlation with the WIO leads to a significant drop in correlation coefficients from 0.80 (lag 0) to 0.58 at lag 3 (see figure 4(b)) showing that at the monthly time scale, the NDVI response to WIO SST is near simultaneous. Correlations with other ENSO indicators at zero-lag, are rather low (see table 1). However, at the 1–4 month lag, there is a significant increase in correlations, for example to -0.80 with NINO3.4 with NDVI lagging NINO3.4 SST by about three months (figure 4(c, d)). Although convective activity was already enhanced in the eastern Pacific by August 1997, the corresponding pattern does not show up in the WIO until October–December during the short rains growing season in East Africa (Bell and Halpert 1998). This is not unexpected as the Indian Ocean response to El Niño involves basin scale warming with a lag of about one season (Cadet and Diehl 1984). This in part accounts for the lagged response between NDVI over East Africa and NINO3.4 SST anomalies.

The Namibia sample site shows a positive relationship with NINO3.4 SST from September to November (figure 4(e)), but this gives way to an inverse relationship in December, and February to May during the late phase of eastern Pacific warming (figure 4(e)). Correlations with most of the ENSO and other interannual variability indicators are rather weak (see table 1). The highest coefficient of correlation is with NINO3.4 at 0.50. The temporal evolution pattern with NINO3.4 SST for south-eastern South Africa is shown in figure 4(f). As in the previous case, the minimum in NDVI is from December to March, corresponding to the period of peak warming in the eastern Pacific. The highest correlations are with SOI (0.43) and WIO-SST (0.43). At the two-month lag the coefficient of correlation with NINO3.4 increases significantly to -0.75 ($p < 0.005$). Although correlations with the QBO and Atlantic SSTs were not significant for the two Southern Africa sites, previous work by Mason and Tyson (1992) and Jury and Pathack (1993) show that the phase of QBO and Atlantic Ocean SSTs can modulate the effects of ENSO over the Southern Africa region. When the QBO is in an anti-SOI phase as was the case during this period, it has a tendency to dampen the normal ENSO drought impacts over Southern

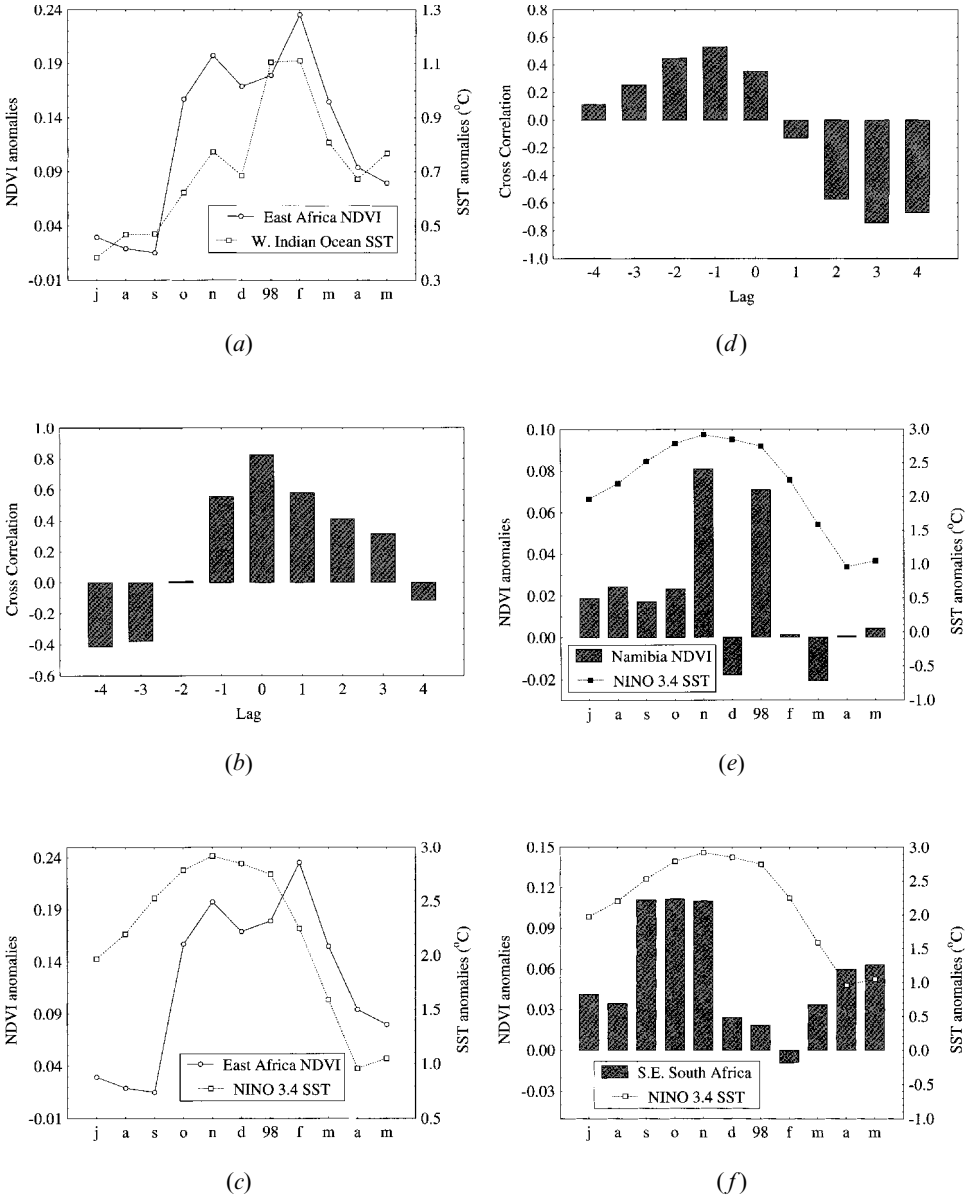


Figure 4. Comparison and correlations between NDVI anomalies and ENSO indices. East Africa (a–d), Southern Africa (e–f). NDVI anomalies over East Africa closely follow the pattern of SST departure patterns in the WIO region (a), with a significant coefficient of correlation at lag 0 ($r = 0.83$) (b). There is an apparent lag of about three months between East Africa NDVI and NINO3.4 SST, with a peak in NINO3.4 SST in December 1997 followed by a peak in East Africa NDVI in February 1998 (c). The lag correlation plot is shown in (d). Shown in (e) and (f) are NDVI anomalies for Namibia and south-eastern South Africa, respectively, plotted against NINO3.4 SST anomalies. In both cases, in the early phase of the event there are slightly positive NDVI anomalies, followed by near normal to negative NDVI anomalies at the maximum of Pacific warming in December–March. This is a recognized feature of rainfall patterns in this region during ENSO warm events with tendency for precipitation to be above normal during the early phase and below normal during the mature phase (Nicholson and Entekhabi 1986).

Table 1. Zero lag correlations between NDVI anomalies for East Africa, Namibia and south-eastern South Africa with various ENSO indices. Correlations marked in bold are significant at $p < 0.005$.

	Variable/ENSO indices							
	NINO3.4	SOI	NAT	SAT	TROP	QBO30	EPWI	WIO
East Africa NDVI	0.35	-0.43	0.30	0.83	0.87	-0.40	-0.68	0.83
Namibia NDVI	0.50	-0.05	-0.17	0.06	0.09	0.35	-0.06	0.17
SE South Africa NDVI	0.176	0.43	0.25	-0.14	-0.35	0.35	-0.02	-0.47

Africa. In general, although the drought during this event was not as severe as during previous events, low NDVI values were observed over Southern Africa during the December 1997–March 1998 period, which is supposed to be the period of maximum precipitation in the region (Ropelewski and Halpert 1987, 1989). The spatial patterns and the evolution of NDVI anomalies during this period, correspond well with observed rainfall anomalies and with the general relationship to the ENSO cycle for this region (Bell and Halpert 1998).

4. Summary and conclusions

The 1997/98 ENSO warm event was the strongest event recorded in the 20th century both in terms of the SST departure patterns and the associated magnitude of the climatic anomalies worldwide. In terms of the land biosphere response over Africa, the most anomalous conditions occurred over equatorial Eastern Africa, in a band bounded by 10°N – 10°S . Positive NDVI anomalies covered the region from October 1997 through May 1998 and, thus, by inference, a persistence of above normal rainfall over the entire region. The normal dry season (December–February) recorded high rainfall totals. Correlation results indicate that the above normal NDVI appears to be a direct result of the anomalous positive SSTs in the WIO region ($\sim +3.0^{\circ}\text{C}$ above normal) and a lagged response to eastern Pacific warming. The positive rainfall response over Eastern Africa resulted in the blooming of vegetation in semi and semi-arid areas of the region and improvement in pasture conditions. In some areas, the above normal rainfall resulted in widespread flooding especially along coastal, eastern and north-eastern Kenya and in Somalia, causing extensive damage to property, claiming hundreds of lives and leaving thousands homeless.

The extensive flooding also created the conditions for the outbreak of various diseases including malaria and Rift Valley Fever (Linthicum *et al.* 1999), which affected human and livestock populations over large areas of East Africa. Slightly greener than normal conditions over southern Africa occurred from October to November 1997 but drier than normal conditions prevailed later in the season from January through May 1998, predominantly over the western part of the region. The eastern portion of the region was slightly greener than normal. The magnitudes of the negative NDVI departures over Southern Africa were not as pronounced as during similar ENSO events in the past including 1982/83, 1986/87, 1992/93 and 1995. At the moment, we hypothesize that this could have been in part a direct result of strong equatorial easterly winds dumping excess moisture from a warmer than normal equatorial WIO, thus dampening the expected drought response. In addition, the counteracting influence of the QBO cannot be ruled out as shown by previous research. The magnitude of the warming in the WIO during this period

was unprecedented in recent history and necessitates serious attention. Since the variability in SSTs in both the Indian and Atlantic Oceans influences rainfall over Africa and may exacerbate or dampen the likely teleconnection effects associated with global ENSO manifestation, incorporation of these SSTs in regional ENSO predictions would be a useful early warning tool for Eastern and Southern Africa.

Acknowledgments

This research was funded under EduTech contract NAS5662 and USRA NAS5-98181 and is a contribution to an interagency programme in support of USAID/FEWS.

References

- ANDRES, L., SALAS, W. A., and SKOLE, D., 1994, Fourier analysis of multi-temporal AVHRR data applied to a land cover classification. *International Journal of Remote Sensing*, **15**, 1115–1221.
- ANYAMBA, A., and EASTMAN, J. R., 1996, Interannual variability of NDVI over Africa and its relationship to El Niño/Southern Oscillation. *International Journal of Remote Sensing*, **17**, 2533–2548.
- ASRAR, G., 1989, *Theory and Applications of Optical Remote Sensing*. Wiley Series in Remote Sensing (New York: John Wiley & Sons).
- BELL, G. D., and HALPERT, M. H., 1998, Climate Assessment for 1997. *Bulletin of American Meteorological Society*, **79**(5), 1–50.
- CADET, D. L., and DIEHL, B. C., 1984, Interannual variability of surface fields over the Indian Ocean during recent decades. *Monthly Weather Review*, **112**, 1921–1935.
- CIHLAR, J., ST LAURENT, L., and DYER, J. A., 1991, The relation between normalized difference vegetation index and ecological variables. *Remote Sensing of Environment*, **35**, 279–298.
- DIAZ, H. F., and KILADIS, G. N., 1993, Atmospheric teleconnections associated with the extreme phases of the Southern Oscillation. In *El Niño: Historical and Paleoclimatic Aspects of the Southern Oscillation*, edited by H. F. Diaz and V. Markgraf (New York: Cambridge University Press), pp. 7–28.
- EASTMAN, J. R., and ANYAMBA, A., 1996, Prototypical patterns of ENSO-related drought and drought precursors in Southern Africa. *The Thirteenth Pecora Symposium Proceedings held at Sioux Falls, South Dakota, USA, 20–22 August 1996* (Sioux Falls, South Dakota: USGS).
- EASTMAN, J. R., and FULK, M. A., 1993, Long sequence time series evaluation using standardized principal components analysis. *Photogrammetric Engineering and Remote Sensing*, **53**, 1649–1658.
- FARRAR, T. J., NICHOLSON, S. E., and LARE, A. R., 1994, The influence of soil type on the relationships between NDVI, rainfall, and soil moisture in semiarid Botswana. II. NDVI response to soil moisture. *Remote Sensing of Environment*, **50**, 121–133.
- GRAY, T. I., and TAPLEY, D. B., 1985, Vegetation health: nature's climate monitor. *Advances in Space Research*, **5**, 371–377.
- HASTENRATH, S., 1990, Decadal-scale changes of the circulation in the tropical Atlantic sector associated with the Sahel drought. *International Journal of Climatology*, **10**, 459–472.
- HOLBEN, B., 1986, Characteristics of maximum-value composite images for temporal AVHRR data. *International Journal of Remote Sensing*, **7**, 1417–1434.
- HUETE, A. R., and TUCKER, C. J., 1991, Investigation of soil influences on AVHRR red and near-infrared vegetation index imagery. *International Journal of Remote Sensing*, **12**, 1223–1242.
- JURY, M. R., and PATHACK, B. M. R., 1993, Composite climate patterns associated with extreme modes of summer rainfall over Southern Africa: 1975–1984. *Theoretical and Applied Climatology*, **47**, 137–147.
- JUSTICE, C. O., HOLBEN, B. N., and GWYNNE, M. D., 1986, Monitoring East African vegetation using AVHRR data. *International Journal of Remote Sensing*, **7**, 1453–1474.
- KATZ, R. W., 1988, Use of cross correlations in the search for teleconnections. *Journal of Climatology*, **8**, 241–253.

- KAUFMAN, Y. J., and HOLBEN, B., 1993, Calibration of the AVHRR visible and near-IR bands by atmospheric scattering, ocean glint and desert reflection. *International Journal of Remote Sensing*, **14**, 21–52.
- LAMB, P. J., and PEPLER, R. A., 1991, West Africa. In *Teleconnections Linking Worldwide Climate Anomalies*, edited by M. H. Glantz, R. W. Katz and N. Nicholls (New York: Cambridge University Press), pp. 121–189.
- LAMB, P. J., PEPLER, R. A., and HASTENRATH, S., 1986, Interannual variability in the tropical Atlantic. *Nature*, **322**, 238–240.
- LINDSEY, J. A., 1988, Southern Africa rainfall, the Southern Oscillation and a southern hemisphere semi-annual cycle. *Journal of Climatology*, **8**, 17–30.
- LINTHICUM, K. J., ANYAMBA, A., TUCKER, C. J., KELLY, P. W., MYERS, M. F., and PETERS, C. J., 1999, Climate and satellite indicators to forecast Rift Valley fever epidemics in Kenya. *Science*, **235**, 1656–1659.
- LOS, S. O., 1993, Calibration adjustment of the NOAA AVHRR Normalized Difference Vegetation Index without recourse to Channel 1 and 2 data. *International Journal of Remote Sensing*, **14**, 1907–1917.
- LOS, S. O., JUSTICE, C. O., and TUCKER, C. J., 1994, A global 1° by 1° NDVI data set for climate studies derived from the GIMMS continental NDVI data. *International Journal of Remote Sensing*, **15**, 3519–3546.
- MASON, S. J., and TYSON, P. D., 1992, The modulation of sea surface temperatures and rainfall associations over Southern Africa with solar activity and the Quasi-Biennial Oscillation. *Journal of Geophysical Research*, **97**, 5847–5856.
- MCPHADEN, M. J., 1999, Genesis and evolution of the 1997–98 El Niño. *Science*, **283**, 950–954.
- MYNENI, R. B., LOS, S. O., and TUCKER, C. J., 1995, Satellite-based identification of linked vegetation index and sea surface temperature anomaly areas from 1982–1990 for Africa, Australia and South America. *Geophysical Research Letters*, **23**, 729–732.
- NICHOLSON, S. E., DAVENPORT, M. L., and MALO, A. R., 1990, A comparison of vegetation response to rainfall in the Sahel and East Africa using Normalized Difference Vegetation Index from NOAA-AVHRR. *Climate Change*, **17**, 209–241.
- NICHOLSON, S. E., and ENTEKHABI, D., 1986, The quasi-periodic behavior of rainfall variability in Africa and its relationship to the Southern Oscillation. *Archive für Meteorologie Geophysik und Bioklimatologie*, **A 34**, 311–348.
- NICHOLSON, S. E., and KIM, J. Y., 1997, The relationship between El Niño-Southern Oscillation to African rainfall. *International Journal of Climatology*, **17**, 117–135.
- OGALLO, L. J., 1988, Relationships between seasonal rainfall in East Africa and the Southern Oscillation. *Journal of Climatology*, **8**, 31–43.
- RASMUSSEN, E. M., and CARPENTER, T. H., 1982, Variations in tropical sea surface temperature and surface wind fields associated with Southern Oscillation / El Niño. *Monthly Weather Review*, **110**, 354–384.
- RICHARD, Y., and POCARD, I., 1998, A statistical study of NDVI sensitivity to seasonal and interannual rainfall variations in Southern Africa. *International Journal of Remote Sensing*, **19**, 2907–2920.
- ROPELEWSKI, C. F., and HALPERT, M. S., 1987, Global and regional scale precipitation patterns associated with El Niño/Southern Oscillation. *Monthly Weather Review*, **115**, 1606–1626.
- ROPELEWSKI, C. F., and HALPERT, M. S., 1989, Precipitation patterns associated with the high-index phase of the Southern Oscillation. *Journal of Climate*, **2**, 268–284.
- ROPELEWSKI, C. F., and HALPERT, M. S., 1996, Quantifying Southern Oscillation-precipitation relationships. *Journal of Climate*, **9**, 1043–1059.
- SAJI, N. H., GOSWAMI, B. N., VINAYACHANDRAN, P. N., and YAMAGATA, T., 1999, A dipole mode in the tropical Indian Ocean. *Nature*, **401**, 360–363.
- SELLERS, P. J., 1985, Canopy reflectance, photosynthesis and transpiration. *International Journal of Remote Sensing*, **8**, 1335–1372.
- TUCKER, C. J., 1979, Red and photographic infrared linear combinations for monitoring vegetation. *Remote Sensing of Environment*, **8**, 127–150.
- TUCKER, C. J., and NEWCOMB, W. W., 1994, AVHRR data sets for determination of desert spatial extent. *International Journal of Remote Sensing*, **17**, 3547–3565.
- TUCKER, C. J., and SELLERS, P. J., 1986, Satellite remote sensing of primary production. *International Journal of Remote Sensing*, **7**, 1133–1135.